

Strain tuning of the nonlinear anomalous Hall effect in MoS₂ monolayer

Yuebei Xiong,[†] Zhirui Gong,^{*,†} and Hao Jin^{*,‡}

[†]*Institute of Quantum Precision Measurement, College of Physics and Optoelectronic Engineering, Shenzhen University, Shenzhen 518060, China*

[‡]*College of Physics and Optoelectronic Engineering, Shenzhen University, Shenzhen 518060, P. R. China*

E-mail: gongzr@szu.edu.cn; jh@szu.edu.cn

Abstract

Due to the time reversal symmetry, the linear anomalous Hall effect (AHE) usually vanishes in MoS₂ monolayer. In contrast, the nonlinear AHE plays an essential role in such system when the uniaxial strain breaks the C_{3v} symmetry and eventually results in the nonzero Berry curvature dipole (BCD). We find that not only the magnitude of the AHE but also the nonlinear Hall angle can be tuned by the strain. Especially the nonlinear Hall angle exhibits a deep relationship which is analogy to the birefracton phenomenon in optics. It actually results from the pseudotensor nature of the BCD moment. Besides the ordinary positive and negative crystals in optics, there are two more birefracton-like cases corresponding to an imaginary refraction index ratio in monolayer MoS₂. Our findings shed lights on the strain controlled electronic devices based on the two-dimensional (2D) materials with BCD.

The Berry phase of the electronic wave function plays a profound role on material properties.^{1,2} The adoption of the Berry curvature (BC) concept establishes the link between the topological nature of electron motion and the intriguing phenomena such as spin/valley Hall effects,³⁻⁶ optical selection rules^{7,8} and magnetoelectric effects.⁹⁻¹¹ Among these phenomena, the various Hall effects are exclusively studied, which facilitates the manipulation of the elec-

tronic currents with different degree of freedoms such as charge, spin and valley indices.^{12,13} In two-dimensional (2D) materials without external magnetic field, only the out-of-plane part of the BC survives, which leads to a simple form of the anomalous Hall effect (AHE).¹⁴ Since the first order Hall conductivity vanishes in time-reversal symmetric crystals, the second order one should be taken into consideration profoundly relating to the Berry curvature dipole (BCD),¹⁵ whose definition is the first-order moment of the BC over the occupied electronic states.¹⁶ It has been studied in various systems such as 2D system,¹⁷⁻²⁵ the Moire superlattice²⁶ and the disorder system.²⁷ Different nonlinear currents such as the nonlinear Hall currents and the optical Hall currents are investigated based on the relaxation time approximation.²⁸ For the highly symmetric system, higher order of the nonlinear AHE are also taken into consideration.^{29,30} In contrast to the scalar linear Hall conductivity requiring the time-reversal broken, the nonlinear Hall conductivity is a pseudotensor and can survive in the solid even possessing the time-reversal symmetry.³¹⁻³³

Recently, the 2D transition metal dichalcogenides (TMDs) monolayer such as MoS₂ attract a lot interest according to their unique electronic and optical properties in the 2D limit and promising application prospects.³⁴⁻³⁶ As a naturally spatial inversion symmetry broken system, there are quite a lot of intriguing phe-

nomena relating to the nonzero BC.³⁷ The nonlinear AHE also vanishes in such system because under the C_{3v} symmetry the BCD is exactly zero. In this sense, the uniaxial strain plays an essential role to achieve considerable nonlinear AHE. Moreover, in contrast with the linear Hall angle which is fixed at 90 degrees, the nonlinear Hall angle can be tuned by the strength of the strain and the orientation of the strain axis.^{38–40} However, the hidden relationship between the nonlinear Hall angles, the orientation of uniaxial strain and the orientation of the ac electric field has not been revealed yet.

Here, we study the uniaxial strain tuned nonlinear AHE in the MoS₂ monolayer. By applying ac electric field and the uniaxial strain, the nonlinear AHE can be achieved in such system. We find that the nonlinear Hall angle, the orientation of the strain axis and the orientation of the ac electric field exhibit a deep relationship which is analogy to the birefracton phenomenon in optics. The orientation of the ac electric field and the nonlinear Hall angle plays the roles as the ordinary and the extraordinary lights in the optical counterparts. Just like the birefracton resulting from the dielectric constant tensor, the hidden relationship between the nonlinear Hall angles, the orientation of the strain and the ac electric field can be established due to the pseudotensor nature of the BCD. In this sense, there are effective refraction indices for these birefracton-like phenomenon in MoS₂. Besides the ordinary positive and negative crystals in optics, we also find that there are two more birefracton-like cases corresponding to imaginary refraction indices in monolayer MoS₂ when accurately tuning the uniaxial strain. Our findings can be generalized to other 2D systems and shed lights on the strain tuning electronic devices based on the 2D materials.

We focus on the origin of nonlinear AHE in the 2D TMDs monolayer, e.g., MoS₂ monolayer. The crystal structure of MoS₂ monolayer is depicted in Fig. 1(a). They are in trigonal prismatic coordination including a Mo atom and two S atoms, which is depicted in Fig. 1(b). The primitive cell of MoS₂ monolayer shows the breaking of spatial inversion symmetry appar-

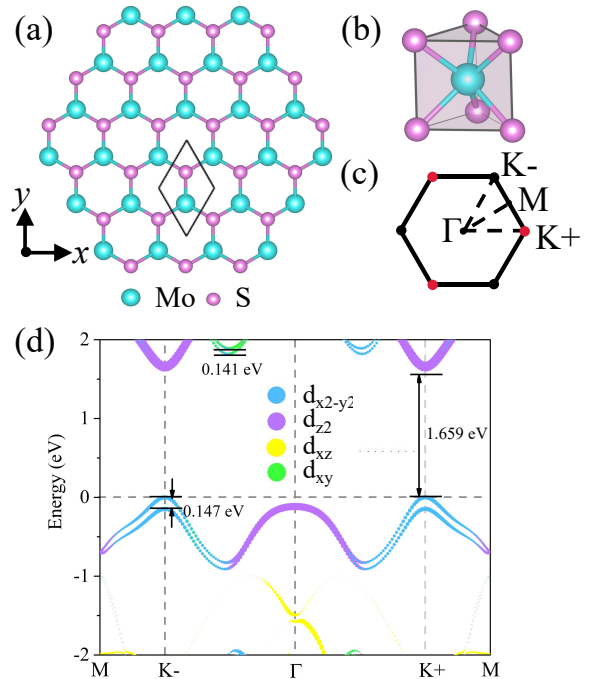


Figure 1: (a) The top view of MoS₂ monolayer. The diamond region shows the 2D primitive cell. (b) The schematic for the structure of trigonal prismatic coordination. (c) The 2D first Brillouin zone with special k points. The two inequivalent valleys K+ and K- and their equivalent counterparts are shown in red and black respectively. (d) The band structure of monolayer MoS₂ with SOC. Contributions from Mo d orbitals: blue dots for $d_{x^2-y^2}$, purple dots for d_{z^2} , yellow dots for d_{xz} , green dots for d_{xy} .

ently. The direct band gaps of MoS₂ monolayer are located at K+ and K- valleys. The Bloch states of MoS₂ monolayer near the band edges mostly consist of Mo 4d orbitals, especially the d_{xy} , $d_{x^2-y^2}$, and d_{z^2} orbitals, which are dominant components for conduction bands (CB) and valence bands (VB). The effective Hamiltonian up to the nearest-neighbor hopping⁴¹

$$H = I_2 \otimes H_0 + H_{soc} + H_{strain} \quad (1)$$

contains three parts: the k.p Hamiltonian of d-orbital electron H_0 , the SOC term H_{soc} and the strain induced term H_{strain} . The first term

$$H_0 = \begin{bmatrix} \frac{\Delta}{2} + \varepsilon & at(q_x\tau - iq_y) \\ at(q_x\tau + iq_y) & -\frac{\Delta}{2} + \varepsilon \end{bmatrix} \quad (2)$$

describes a massive Dirac electron, where Δ is the band gap, ε is the correction energy bound up with the Fermi energy, a is the lattice constant, t is the hopping constant and $\vec{q} = (q_x, q_y)$ is the momentum vector. Here, the CB and the VB are respectively dominantly composed of d_{z^2} orbital and d_{-2} orbital, where $d_{-2} = \frac{1}{\sqrt{2}}(d_{x^2-y^2} - id_{xy})$. The valley dependent SOC term is written as

$$H_{soc} = \tau\sigma_z \otimes \begin{bmatrix} \lambda_c & 0 \\ 0 & \lambda_v \end{bmatrix}, \quad (3)$$

where τ is the valley index, σ_z is the z component Pauli matrix, λ_c (λ_v) represents the effective SOC splitting in the band edge of CB and VB. The band structure of MoS₂ monolayer is depicted in Fig. 1(d). The energy splitting between the majority spin of the valence band maximum (VBM) and the minority spin of the VBM is up to $2\lambda_v = 147$ meV. In contrast, The energy splitting between the majority spin and the minority spin of the conduction band minimum (CBM) is $2\lambda_c \sim 0$ meV.

Usually, BCD is non-zero in a crystal if the inversion symmetry is broken. However, the C_{3v} symmetry of the crystal forces the BCD to vanish. The strain-induced term $H_{strain} = \tau at \vec{\alpha} \cdot \vec{q}$ is introduced to break the C_{3v} symmetry, where $\vec{\alpha} = (u_{xx} - u_{yy}, -2u_{xy})$ containing both the uniaxial and the shear strain and $u_{ij} = (\partial_i u_j + \partial_j u_i)/2$ are the in-plane deformations. It can arise when applying uniaxial strain in the zigzag direction.⁴² Here, we have ignored the strain induced isotropic and anisotropic position-dependent Fermi velocity in comparison with free Fermi velocity in H_0 .⁴⁰

The nonlinear currents need to be taken into consideration which exactly result from the BCD. In the former references^{15,16,18,20} only the scalar part of the BCD is considered which gives rise to nonlinear current as $j_a^n = \Re[\chi_{acd}(e^{2i\omega t} + 1)] E_c E_d$. Here, the superscript n stands for nonlinear, $a, c, d = x, y$ are the in plane directions, $\mathbf{E}(t) = (E_x \mathbf{x} + E_y \mathbf{y}) e^{i\omega t}$ is the ac electric field with frequency ω . Here, \mathbf{x} and \mathbf{y} are respectively the unit vector along x and y directions, E_x and E_y are the corresponding

electric field strengths.

Based on the relaxation time approximation of the electron distribution, the Langevin equation with the relaxation time τ_0 can be written as

$$\frac{\partial f}{\partial t} = \frac{e}{\hbar} E_a(t) \partial_a f - \frac{1}{\tau_0} (f - f_0). \quad (4)$$

Here, $E_a(t)$ is the component of the ac electric field along a direction, where $a = (x, y)$, and f_0 is the Fermi distribution without the ac electric field. The nonlinear conductivities are given as

$$\chi_{acd} = -\epsilon_{abc} \frac{e^3 \tau}{2(1 + i\omega\tau)} D_d, \quad (5)$$

with $D_d = \int \partial_d \Omega_b(\mathbf{k}) f_0(\mathbf{k}) \frac{d\mathbf{k}}{(2\pi)^2}$. Here, the BC is straightforwardly obtained as

$$\Omega_b(\mathbf{q} \pm \mathbf{K}) = \pm \frac{2a^2 t^2 (\Delta - \lambda_v)}{[4a^2 t^2 q^2 + (\Delta - \lambda_v)^2]^{\frac{3}{2}}}, \quad (6)$$

and

$$\partial_d \Omega_b(\mathbf{q} \pm \mathbf{K}) = \mp \frac{24a^4 q_d t^4 (\Delta - \lambda_v)}{[4a^2 t^2 q^2 + (\Delta - \lambda_v)^2]^{\frac{5}{2}}}. \quad (7)$$

The BC is depicted in Fig. 2(b), where obviously the BC is opposite in the opposite valleys. Here, $b = z$ for the 2D materials and ϵ_{abc} is the Levi-Civita symbol. In this sense, the only four surviving elements of the nonlinear conductivity tensor are $\chi_{xyx} = -\chi_{yxx}$ and $\chi_{xyy} = -\chi_{yyx}$. Apparently, χ_{xyx} and χ_{xyy} are real ones in the Drude limit $\omega\tau \ll 1$. Since D_x related to $\partial_x \Omega$ which is anti-symmetric along x direction, the D_x is nonzero when the Dirac cone is tilted along x direction as shown in Fig. 2(a). In this sense, D_x is independent of the strain along y direction, and accordingly D_y is independent of the strain along x direction.

The nonlinear current vanishes when no strain is applied because $\partial_d \Omega_b(\mathbf{k})$ is odd function as $\partial_d \Omega_b(\mathbf{q} \pm \mathbf{K}) = -\partial_d \Omega_b(-\mathbf{q} \pm \mathbf{K})$ while Fermi distribution is even one as $f_0(\mathbf{q} \pm \mathbf{K}) = f_0(-\mathbf{q} \pm \mathbf{K})$. The $\partial_d \Omega_b(\mathbf{k})$ with and without applying the strain in different valleys are depicted in Fig. 2(c), where the Kramers degeneracy is quite obvious. When the strain is applied, the $\partial_d \Omega_b(\mathbf{k})$ in the K+ and K- shifted in

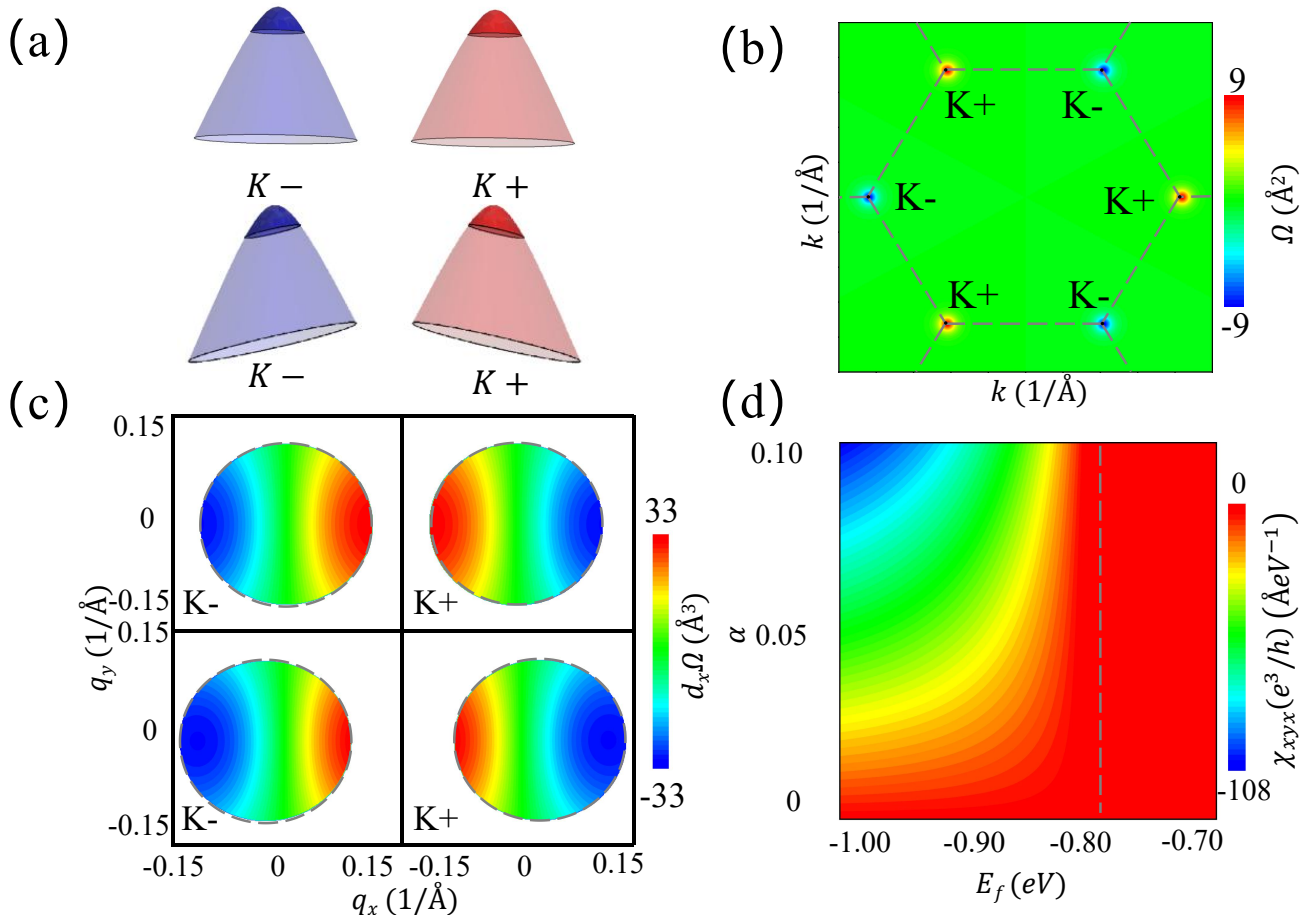


Figure 2: (a) The Fermi pockets without strain and with strain. The darker blue and red parts denote the carrier distribution respectively corresponding to positive and negative BC, which gives rise to the Hall current. In order to obtain the nonzero BCD, the tilted Dirac cone is necessary and can be completely controlled by the strain which can be controlled by the strain. (b) The BC in the first Brillouin zone. (c) The $\partial_x \Omega$ without and with strain in different valleys. The grey dash lines represent the Fermi surface. (d) χ_{xyx} versus E_f and α . The parameters are $\Delta = 1.766$ eV, $a = 3.160$ Å, $E_f = 0.81$ eV, $t = 1.137$ eV, $\lambda_v = 0.73$ meV. The grey dash line represents the Fermi surface.

opposite directions, resulting in a larger BCD, which leads to a respectively large nonlinear Hall current. Therefore the strain plays an essential role in the appearance of the nonlinear current. The nonlinear current vanishes when no strain is applied because BCD is odd function as $\partial_d \Omega_b(\mathbf{q} \pm \mathbf{K}) = -\partial_d \Omega_b(-\mathbf{q} \pm \mathbf{K})$ while Fermi distribution is even one as $f_0(\mathbf{q} \pm \mathbf{K}) = f_0(-\mathbf{q} \pm \mathbf{K})$. The large magnitude of the nonlinear current results from the long relaxation time $\tau_0 \sim 1ps$.⁴³ The χ_{xyx} versus E_f and α is shown in Fig. 2(d), the χ_{xyx} decreases when increasing the strain strength α for a fixed Fermi surface $E_f < E_{VBM}$. The similar relationship

appears in χ_{xyy} , which depends on the strain strength β in y direction.

The corresponding nonlinear current $\mathbf{j} = (j_x, j_y)$ is given in the matrix form as

$$\begin{bmatrix} j_x \\ j_y \end{bmatrix} = \Re \left[(e^{2i\omega t} + 1) \overleftrightarrow{\chi} \begin{bmatrix} E_x^2 \\ 2E_x E_y \\ E_y^2 \end{bmatrix} \right] \quad (8)$$

the pseudotensor $\overleftrightarrow{\chi} = \begin{bmatrix} 0 & \chi_{xyx} & \chi_{xyy} \\ -\chi_{xyx} & -\chi_{xyy} & 0 \end{bmatrix}$. The nonlinear Hall angle is defined by $\theta_{non} = j_y/j_x$, which demonstrates the propagation direction of the nonlinear AHE. By defining the orientation of the ac electric field and the ori-

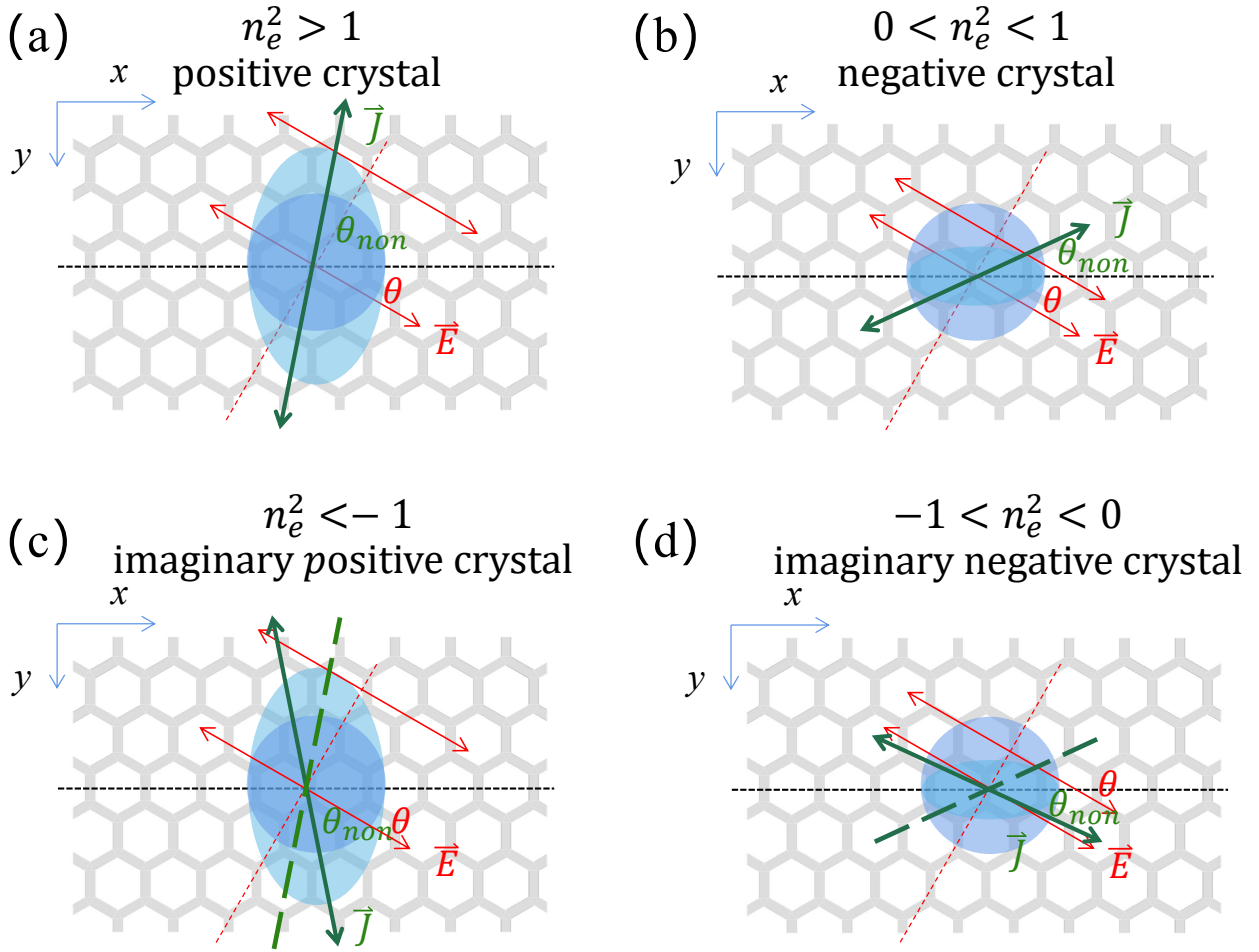


Figure 3: Propagation direction of the nonlinear current determined by the Huygens' Principle for different n_e^2 . Here, The red arrow and darker green arrows represent the polarization direction of the electric field and the propagation direction of the nonlinear current. The darker green dash lines represents the direction of the nonlinear current in (a) and (b) respectively.

entation of the strain $\tan \theta = E_y/E_x = \alpha/\beta$ and $\tan \phi = D_x/D_y$, the nonlinear Hall angle is straightforwardly obtained as $\tan \theta_{non} = (-\cot \theta) n_e^2$ with

$$n_e^2 = \frac{\tan \phi + 2 \tan \theta}{2 \tan \phi + \tan \theta}. \quad (9)$$

Here, D_x and D_y is proportional to α and β respectively, and the ratio are equal. $D_x/D_y = \alpha/\beta$ due to the C_{3v} symmetry. In the former references,^{15,18} only the ac electric field along the x direction (y direction) is taken into consideration, which is $\theta = 0$ ($\theta = \pi/2$) and the nonlinear Hall angle is $\theta_{non} = \pi/2$ ($\theta_{non} = 0$) whatever the strain orientation is. However, when the orientation of the ac electric field is

an arbitrary one, the nonlinear Hall angle is tuned both by the orientation of the ac electric field θ and the direction defined by the BCD moments ϕ . Here, n_e actually plays the same role of the refraction index in the birefraction phenomenon in optics. The cartoon of those directions according to the Huygens' Principle is shown in Fig. 3, where the radius of the circle is 1 and the major axis and minor axis of ellipse are 1 and $|n_e|$ respectively. The $n_e^2 > 1$ (Fig. 3(a)) and $0 < n_e^2 < 1$ (Fig. 3(b)) correspond to the positive and negative crystals for the birefraction phenomenon. Besides these ordinary cases, $n_e^2 < -1$ (Fig. 3(c)) and $-1 < n_e^2 < 0$ (Fig. 3(d)) also exist, which have no optical counterparts since the refraction indices become imaginary in these two cases. The

θ_{non} in imaginary positive crystal (imaginary negative crystal) is equal in magnitude, but opposite in sign with θ_{non} in positive crystal (negative crystal).

We provide the phase diagram of n_e^2 versus θ and ϕ in Fig. 4. The blue, yellow, red and green areas represent positive crystal (P), negative crystal (N), the imaginary positive crystal (IP) and imaginary negative crystal (IN) phases. As we can see, if θ and ϕ are switched, n_e^2 becomes the reciprocal of itself, and eventually the negative phases and the positive phases are correspondingly switched.

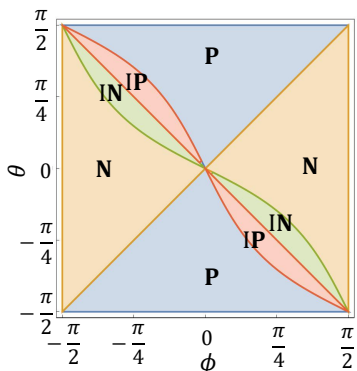


Figure 4: The phase diagram of n_e^2 versus θ and ϕ . The blue, yellow, red and green areas represent positive crystal (P), negative crystal (N), the imaginary positive crystal (IP) and imaginary negative crystal (IN) phases.

In conclusion, we study the uniaxial strain tuned nonlinear AHE in the MoS₂ monolayer. By applying ac electric field and the uniaxial strain, the nonlinear AHE can be achieved in such system. We find that not only the magnitude of the nonlinear AHE but also the nonlinear Hall angle can be tuned by the strain. The nonlinear Hall angle, the orientation of the strain axis and the orientation of the ac electric field exhibit a deep relationship which is analogy to the birefracton phenomenon in optics. The orientation of the ac electric field and the nonlinear Hall angle play the roles as the ordinary and the extraordinary lights in the optical counterparts. Just like the birefracton resulting from the dielectric constant tensor, the hidden relationship between the orientation of the ac electric field and nonlinear Hall angles can be established due to the pseudotensor nature

of the BCD. In this sense, there are effective refraction indices for these birefracton-like phenomenon in MoS₂. Besides the ordinary positive and negative crystals in optics, we also find that there are two more birefracton-like cases corresponding to an imaginary refraction index in MoS₂ monolayer when accurately tuning the uniaxial strain. Our findings can be generalized to other 2D systems and shed lights on the strain tuning electronic devices based on the 2D materials.

Method

The band structure of MoS₂ was calculated using first-principles simulations within density functional theory (DFT). The projected augmented wave pseudopotentials method was used as implemented in the Vienna *Ab initio* Simulation Package (VASP). The exchange correlation energy was calculated using the generalized gradient approximation (GGA) of the Perdew-Burke-Ernzerhof form, and the plane wave cutoff energy was set to 500 eV. For the calculation of band structure, a centered 21 x 21 x 1 kpoint mesh was used. The vacuum space along the z direction was set to be > 20 Å. The plane lattice constant and atomic coordinates were fully relaxed until the energy and force converged to 10^{-8} and 10^{-2} eV/Å, respectively.

Acknowledgement This work was supported by NSFC Grants No. 12175150 and Guangdong Basic and Applied Basic Research Foundation (Grant No. 2022A1515012006 and 2023A1515011223.).

References

- (1) X. Gu, A. F. Kockum, A. Miranowicz, Y.-X. Liu, and F. Nori, “Microwave photonics with superconducting quantum circuits,” *Phys. Rep.*, **718**, 1–102 (2017).
- (2) D. Xiao, M.-C. Chang, and Q. Niu, “Berry phase effects on electronic properties,” *Rev. Mod. Phys.*, **82**, 1959–2007 (2010).

- (3) D. Xiao, W. Yao, and Q. Niu, “Valley-contrasting physics in graphene: magnetic moment and topological transport,” *Phys. Rev. Lett.*, **99**, 236809 (2007).
- (4) D. Xiao, G.-B. Liu, W. Feng, X. Xu, and W. Yao, “Coupled spin and valley physics in monolayers of MoS₂ and other group-VI dichalcogenides,” *Phys. Rev. Lett.*, **108**, 196802 (2012).
- (5) Y. K. Kato, R. C. Myers, A. C. Gossard, and D. D. Awschalom, “Observation of the spin Hall effect in semiconductors,” *Science*, **306**, 1910–1913 (2004).
- (6) J. Wunderlich, B. Kaestner, J. Sinova, and T. Jungwirth, “Experimental observation of the spin-Hall effect in a two-dimensional spin-orbit coupled semiconductor system,” *Phys. Rev. Lett.*, **94**, 047204 (2005).
- (7) W. Yao, D. Xiao, and Q. Niu, “Valley-dependent optoelectronics from inversion symmetry breaking,” *Phys. Rev. B*, **77**, 235406 (2008).
- (8) I. Souza and D. Vanderbilt, “Dichroic f-sum rule and the orbital magnetization of crystals,” *Phys. Rev. B*, **77**, 054438 (2008).
- (9) Z. Gong, G.-B. Liu, H. Yu, D. Xiao, X. Cui, X. Xu, and W. Yao, “Magnetoelectric effects and valley-controlled spin quantum gates in transition metal dichalcogenide bilayers,” *Nat. Commun.*, **4**, 2053 (2013).
- (10) G. Aivazian, Z. Gong, A. M. Jones, R.-L. Chu, J. Yan, D. G. Mandrus, C. Zhang, D. Cobden, W. Yao, and X. Xu, “Magnetic control of valley pseudospin in monolayer WSe₂,” *Nat. Phys.*, **11**, 148–152 (2015).
- (11) A. Srivastava, M. Sidler, A. V. Allain, D. S. Lembke, A. Kis, and A. Imamoglu, “Valley Zeeman effect in elementary optical excitations of monolayer WSe₂,” *Nat. Phys.*, **11**, 141–147 (2015).
- (12) N. Nagaosa, J. Sinova, S. Onoda, A. H. MacDonald, and N. P. Ong, “Anomalous Hall effect,” *Rev. Mod. Phys.*, **82**, 1539–1592 (2010).
- (13) M. I. Dyakonov and A. V. Khaetskii, “Spin Hall effect,” in *Spin Physics in Semiconductors*, pp. 211–243, Springer, 2008.
- (14) J. Lai, J. Zhan, P. Liu, X.-Q. Chen, and Y. Sun, “Electric field tunable nonlinear Hall terahertz detector in the dual quantum spin Hall insulator TaIrTe₄,” *Phys. Rev. B*, **110**, 155122 (2024).
- (15) I. Sodemann and L. Fu, “Quantum nonlinear Hall effect induced by Berry curvature dipole in time-reversal invariant materials,” *Phys. Rev. Lett.*, **115**, 216806 (2015).
- (16) Z. Zhang, Z.-G. Zhu, and G. Su, “Theory of nonlinear response for charge and spin currents,” *Phys. Rev. B*, **104**, 115140 (2021).
- (17) A. Naseer, A. Priyadarshi, P. Ghosh, R. Ahammed, Y. S. Chauhan, S. Bhowmick, and A. Agarwal, “Room temperature ferroelectricity and an electrically tunable Berry curvature dipole in III–V monolayers,” *Nanoscale*, (2024).
- (18) G. Kim, J. Bahng, J. Jeong, W. Sakong, T. Lee, D. Lee, Y. Kim, H. Rho, and S. C. Lim, “Gate modulation of dissipationless nonlinear quantum geometric current in 2D Te,” *Nano Lett.*, **24**, 10820–10826 (2024).
- (19) L. Wang, J. Zhu, H. Chen, H. Wang, J. Liu, Y.-X. Huang, B. Jiang, J. Zhao, H. Shi, G. Tian, *et al.*, “Orbital magneto-nonlinear anomalous Hall effect in kagome magnet Fe₃Sn₂,” *Phys. Rev. Lett.*, **132**, 106601 (2024).
- (20) N. Kheirabadi and A. Langari, “Quantum nonlinear planar Hall effect in bilayer graphene: An orbital effect of a steady in-plane magnetic field,” *Phys. Rev. B*, **106**, 245143 (2022).

- (21) R. Habara and K. Wakabayashi, “Non-linear optical Hall effect of few-layered NbSe₂,” *Phys. Rev. Res.*, **4**, 013219 (2022).
- (22) S. S. Samal, S. Nandy, and K. Saha, “Non-linear transport without spin-orbit coupling or warping in two-dimensional Dirac semimetals,” *Phys. Rev. B*, **103**, L201202 (2021).
- (23) J. Li, H. Jin, Y. Wei, and H. Guo, “Tunable intrinsic spin Hall conductivity in bilayer PtTe₂ by controlling the stacking mode,” *Phys. Rev. B*, **103**, 125403 (2021).
- (24) H. Jin, H. Su, X. Li, Y. Yu, H. Guo, and Y. Wei, “Strain-gated nonlinear Hall effect in two-dimensional MoSe₂/WSe₂ van der Waals heterostructure,” *Phys. Rev. B*, **104**, 195404 (2021).
- (25) J.-S. You, S. Fang, S.-Y. Xu, E. Kaxiras, and T. Low, “Berry curvature dipole current in the transition metal dichalcogenides family,” *Phys. Rev. B*, **98**, 121109 (2018).
- (26) L. Du, Z. Huang, J. Zhang, F. Ye, Q. Dai, H. Deng, G. Zhang, and Z. Sun, “Non-linear physics of moiré superlattices,” *Nat. Mater.*, **23**, 1179–1192 (2024).
- (27) R. Chen, Z. Z. Du, H.-P. Sun, H.-Z. Lu, and X. C. Xie, “Nonlinear Hall effect on a disordered lattice,” *Phys. Rev. B*, **110**, L081301 (2024).
- (28) M.-S. Qin, P.-F. Zhu, X.-G. Ye, W.-Z. Xu, Z.-H. Song, J. Liang, K. Liu, and Z.-M. Liao, “Strain tunable Berry curvature dipole, orbital magnetization and nonlinear Hall effect in WSe₂ monolayer,” *Chin. Phys. Lett.* **38**, 017301 (2021).
- (29) C.-P. Zhang and K. T. Law, “Nonlinear Hall effect in an insulator,” *Nat. Nanotechnol.*, **19**, 1432–1433 (2024).
- (30) C.-P. Zhang, X.-J. Gao, Y.-M. Xie, H. C. Po, and K. T. Law, “Higher-order nonlinear anomalous Hall effects induced by Berry curvature multipoles,” *Phys. Rev. B*, **107**, 115142 (2023).
- (31) C. Ortix, “Nonlinear Hall Effect with Time-Reversal Symmetry: Theory and Material Realizations,” *Adv. Quantum Technol.*, **4**, 2100056 (2021).
- (32) K. Das, K. Ghorai, D. Culcer, and A. Agarwal, “Nonlinear valley Hall effect,” *Phys. Rev. Lett.*, **132**, 096302 (2024).
- (33) Z. Z. Du, C. M. Wang, H. P. Sun, H. Z. Lu, and X. C. Xie, “Quantum theory of the nonlinear Hall effect,” *Nat. Commun.*, **12**, 5038 (2021).
- (34) H. Zeng, J. Dai, W. Yao, D. Xiao, and X. Cui, “Valley polarization in MoS₂ monolayers by optical pumping,” *Nat. Nanotechnol.* **7**, 490 (2012).
- (35) K. F. Mak, K. He, J. Shan, and T. F. Heinz, “Control of valley polarization in monolayer MoS₂ by optical helicity,” *Nat. Nanotechnol.* **7**, 494 (2012).
- (36) A. M. Jones, H. Yu, N. J. Ghimire, S. Wu, G. Aivazian, J. S. Ross, B. Zhao, J. Yan, D. G. Mandrus, D. Xiao, *et al.*, “Optical generation of excitonic valley coherence in monolayer WSe₂,” *Nat. Nanotechnol.* **8**, 634 (2013).
- (37) T. Cao, G. Wang, W. Han, H. Ye, C. Zhu, J. Shi, Q. Niu, P. Tan, E. Wang, B. Liu, *et al.*, “Valley-selective circular dichroism of monolayer molybdenum disulfide,” *Nat. Commun.* **3**, 887 (2012).
- (38) Y. Araki, “Strain-induced nonlinear spin Hall effect in topological Dirac semimetal,” *Sci. Rep.*, **8**, 15236 (2018).
- (39) J. Wan, Y.-L. Wu, K.-Q. Chen, and X.-Q. Yu, “Strongly enhanced nonlinear acoustic valley Hall effect in tilted Dirac materials,” *Phys. Rev. B*, **109**, L161101 (2024).
- (40) P. A. Pantalen, T. Low, and F. Guinea, “Tunable large Berry dipole in strained twisted bilayer graphene,” *Phys. Rev. B* **103**, 205403 (2021).

- (41) D. Xiao, G.-B. Liu, W. Feng, X. Xu, and W. Yao, "Coupled spin and valley physics in monolayers of MoS₂ and other group-VI dichalcogenides," *Phys. Rev. Lett.* **108**, 196802 (2012).
- (42) P. A. Pantalen, T. Low, and F. Guinea, "Tunable large Berry dipole in strained twisted bilayer graphene," *Phys. Rev. B* **103**, 205403 (2021).
- (43) H. Wang, C. Zhang, and F. Rana, "Surface recombination limited lifetimes of photoexcited carriers in few-layer transition metal dichalcogenide MoS₂," *Nano Lett.* **15**, 8204 (2015).